PHILOSOPHICAL MAGAZINE, 2003, VOL. 83, NO. 8, 1045–1057

Electron-optical phase shift of magnetic nanoparticles I. Basic concepts

M. BELEGGIA† and Y. ZHU

Materials Science Department, Brookhaven National Laboratory, Upton, New York 11973, USA

[*Received 25 September 2002 and accepted 9 November 2002*]

ABSTRACT

The electron-optical phase shift induced in the electron beam due to the interaction with the electromagnetic field of magnetized nanoparticles of defined shape and arbitrary dimensions is calculated, presented and discussed. Together with the computable knowledge of vector potential and magnetic induction, including the demagnetizing field, and with the extension to more realistic geometries which will be presented in part II, this theoretical framework can be employed for the interpretation of transmission electron microscopy experiments on magnetic particles on the nanometre scale.

§1. INTRODUCTION

Magnetic structures on the nanometre scale are of fundamental importance from both the scientific and the technological point of view. As the standard techniques for characterization, such as magnetic force microscopy (Gomez 2001), spin-polarized scanning electron microscopy (Unguris 2001) and scanning transmission electron microscopy (Chapman 1984), are close to their limits owing to the small length scale involved, transmission electron microscopy (TEM) represents the most promising candidate for the high-spatial-resolution characterization of advanced technological materials (De Graef 2001).

The magnetic signal of the material is encoded in the electron wave in terms of a phase shift. Many techniques are now available for retrieval of the electron-optical phase shift, in particular electron holography (Tonomura 1993) and the transport-of-intensity equation (Paganin and Nugent 1998). However, since the interpretation of the wave modulation is not straightforward, accurate modelling, followed by a thorough analysis of the recorded experimental results, is always required.

A good amount of literature is available in dealing with magnetized particles, or magnetic domains (for example De Graef *et al*. 1999). The calculation of the magnetic properties, analytical or numerical, is generally feasible, and examples applied to the problem can be found in electromagnetism textbooks (for example Jackson 1975). However, regarding electron microscopy and associated phase contrast, one further step is needed to obtain the phase shift, as the integral of the vector potential along the electron trajectory.

† Author for correspondence. Email: beleggia@bnl.gov.

Philosophical Magazine ISSN 1478–6435 print/ISSN 1478–6443 online © 2003 Taylor & Francis Ltd
http://www.tandf.co.uk/journals
DOI: 10.1080/0141861031000066166

In this paper, a basic theoretical framework for the interpretation of images of magnetized nanoparticles with defined geometry, arbitrary dimensions and simple field topography (uniform or circular) will be presented. Following the Fourier space approach recently introduced and successfully employed for the image interpretation of vortices in superconducting materials (Beleggia and Pozzi 2000, 2001), it is now possible, starting from a known magnetization topography, to calculate analytically the corresponding vector potential, magnetic induction, demagnetizing field and electron-optical phase shift, thus providing a complete framework to analyse the experimental data.

By means of the above-mentioned Fourier approach, we generalize the theoretical framework and consider a generic particle shape, geometry and configuration. Whenever it is possible to perform the Fourier transform of the shape function (describing the region of space bounded by the particle surface), the corresponding phase shift can be derived analytically. While in this paper (part I) we limit our investigation to three basic geometries (rectangular, cylindrical and spherical), in the companion paper, part II (Beleggia *et al.* 2003), it will be shown how to calculate the phase shift for a broad class of geometries: the polyhedral (faceted) particles.

The inversion of the Fourier representation of the phase shift to real space is possible only for very simple configurations. However, exploiting the fast Fourier transform (FFT) algorithm, we can handle the phase shift in Fourier space with a negligible increase in computing time.

After brief general considerations, where the Fourier approach will be reviewed and adapted to the present case, it will be shown in this paper how to calculate the phase shift for single-domain magnetic nanoparticles of rectangular, spherical and cylindrical geometry. Then the vortex state of the magnetization will be analysed. In the following, it will be pointed out how the Fourier representation allows us to calculate the phase shift for a generic specimen tilt, and to extend the theoretical framework to periodic arrays of structures. The tilted-specimen set-up enables us to retrieve information about the vertical component of the magnetic field, and to separate the electrostatic and magnetic contributions to the phase shift. The phase shift of a regular array of particles allows us to analyse the magnetic field topography induced by the mutual interaction between packed nanoparticles, the demagnetizing effects depending on the particle geometry, and may also give some hints about physical exchange properties of the structure.

§ 2. Model for magnetic nanoparticles

The expression linking the magnetization and magnetic vector potential, namely

$$\mathbf{A}(\mathbf{r}) = \frac{\mu_0}{4\pi} \int \mathbf{M}(\mathbf{r}') \times \frac{\mathbf{r} - \mathbf{r}'}{|\mathbf{r} - \mathbf{r}'|^3} \, \mathrm{d}^3\mathbf{r}', \tag{1}$$

represents an invaluable resource for the calculation of magnetic configurations starting from a known magnetization. In fact, exploiting the convolution theorem and the linearity of the vector product operation, equation (1) can be written in three-dimensional Fourier space as

$$\mathbf{A}(\mathbf{k}) = \frac{\mu_0}{4\pi} \mathbf{M}(\mathbf{k}) \times \mathcal{F}\left(\frac{\mathbf{r}}{r^3}\right) = -\frac{\mathrm{i}\mu_0}{k^2} \mathbf{M}(\mathbf{k}) \times \mathbf{k}. \tag{2}$$

Hence, the calculation of the vector potential is reduced to a vector product, if the Fourier transform of the magnetization is computable.

In particular cases, such as a semi-infinite array of 180° magnetic domains, we can perform this calculation analytically, and obtain a closed form in terms of special functions for the electron optical phase shift. The details of this calculation have been presented elsewhere (Beleggia *et al*. 2003). In this paper, we focus our attention on the magnetized nanoparticles.

To cover all the possible geometries involved in the experiments, we can start by the three basic configurations, namely rectangular, cylindrical and spherical. As a first approximation, we shall consider uniformly magnetized particles.

In general, we can write the magnetization vector as $M_0\hat{\mathbf{m}}$ for $\mathbf{r}$ inside the particle, and zero outside, introducing the dimensionless shape function $D(\mathbf{r})$ (also called characteristic function) to represent the region of space bounded by the particle surface:

$$\mathbf{M}(\mathbf{r}) = M_0\hat{\mathbf{m}}D(\mathbf{r}). \tag{3}$$

The Fourier transform of equation (3) can be written as

$$\mathbf{M}(\mathbf{k}) = M_0\hat{\mathbf{m}} \int \mathrm{d}^3\mathbf{r}\, D(\mathbf{r}) \exp(-\mathrm{i}\mathbf{k}\cdot\mathbf{r}) = M_0\hat{\mathbf{m}}D(\mathbf{k}), \tag{4}$$

where $D(\mathbf{k})$ is the Fourier transform of the shape function, often called the shape amplitude or shape transform.

From equations (1) and (2) we can calculate directly the vector potential in Fourier space:

$$\mathbf{A}(\mathbf{k}) = -\frac{\mathrm{i}B_0}{k^2} D(\mathbf{k})(\hat{\mathbf{m}} \times \mathbf{k}), \tag{5}$$

where $\mu_0 M_0 = B_0$ is the magnetic induction corresponding to a magnetization M_0.

From knowledge of the vector potential, one can easily calculate the magnetic induction as $\mathbf{B} = \nabla \times \mathbf{A}$, and the phase shift as a line integral along the electron trajectory. Let us first concentrate on the magnetic induction, in order to establish a correspondence between well-known results of electromagnetic theory and our approach.

As any differential operator in real space is a reciprocal vector in Fourier space, the nabla operator becomes $\nabla \rightarrow \mathrm{i}\mathbf{k}$. Therefore, the curl is translated into a vector product as follows:

$$\mathbf{B}(\mathbf{k}) = \mathrm{i}\mathbf{k} \times \mathbf{A}(\mathbf{k}) = \frac{B_0}{k^2} D(\mathbf{k})(\mathbf{k} \times \hat{\mathbf{m}} \times \mathbf{k}), \tag{6}$$

which, exploiting the vector identity $\mathbf{k} \times \hat{\mathbf{m}} \times \mathbf{k} = \hat{\mathbf{m}}k^2 - \mathbf{k}(\mathbf{k}\cdot\hat{\mathbf{m}})$, can also be written, after an inverse Fourier transform, as the sum of the induction proportional to the magnetization and the demagnetizing field:

$$\mathbf{B} = \mu_0\mathbf{M} = \frac{B_0}{8\pi^3} \int \mathrm{d}^3\mathbf{k}\, \frac{D(\mathbf{k})}{k^2}\, \mathbf{k}(\hat{\mathbf{m}}\cdot\mathbf{k}) \exp(\mathrm{i}\mathbf{k}\cdot\mathbf{r}). \tag{7}$$

The integral in equation (7) evaluated in the inner part of a spherical particle yields $-\frac{1}{3}B_0\hat{\mathbf{m}}$, which is exactly the demagnetizing factor for a sphere, for which the relationship $\mathbf{B} = \frac{2}{3}\mu_0\mathbf{M}$ holds. It has been thus demonstrated how the vector potential calculated from equation (1) takes into account also the demagnetizing field

extending in the vacuum surrounding the particle. This field depends on the geometry of the uniformly magnetized particle.

To describe the phase shift induced on the impinging electrons by the electromagnetic field associated with the nanoparticle, we resort to the standard Aharonov–Bohm (1959) expression:

$$\begin{aligned}\varphi(x,y) &= \varphi_{\mathrm{e}} + \varphi_{\mathrm{m}} \\ &= \frac{\pi}{\lambda E}\int V(x,y,z)\,\mathrm{d}z - \frac{\pi}{\phi_0}\int A_z(x,y,z)\,\mathrm{d}z,\end{aligned} \tag{8}$$

where λ is the electron wavelength, E is a parameter with the dimension of energy which depends on the acceleration voltage and ϕ_0 is the flux quantum $h/2e = 2.07 \times 10^3\,\mathrm{T\,nm^2}$.

The electrostatic contribution φ_{e} in equation (8) can be written as

$$\varphi_{\mathrm{e}} = \frac{\pi V_0}{\lambda E}\, t_{\mathrm{p}}, \tag{9}$$

where t_{p} is the projected thickness of the particle and V_0 is the effective mean inner potential, that is the difference between the mean inner potentials of the material and of the medium in which the particle is embedded (the vacuum is considered to be a medium with vanishing mean inner potential).

The magnetic component φ_{m} can be calculated from knowledge of the vector potential. After integration along the z axis, which is performed in Fourier space, we obtain

$$\varphi_{\mathrm{m}}(\mathbf{k}) = \frac{\mathrm{i}\pi B_0}{\phi_0}\,\frac{D(k_x,k_y,0)}{k_\perp^2}\,(\hat{\mathbf{m}}\times\mathbf{k})|_z, \tag{10}$$

where $k_\perp = (k_x^2 + k_y^2)^{1/2}$.

Equation (10) suggests that, in order to calculate the phase shift of a uniformly magnetized nanoparticle, all we need to know is the shape amplitude, together with the direction and intensity of the magnetization.

2.1. *Rectangular geometry*

Let us now consider a rectangular particle with uniform magnetization and lateral dimensions $2L_x$, $2L_y$ and thickness $t = 2d$, as shown in figure 1 (*a*). The most suitable coordinate system in this case is the standard Cartesian reference frame (x, y, z). The shape function $D(\mathbf{r})$ can be expressed as

$$D(\mathbf{r}) = 1 \quad \text{for} \quad |x| < L_x, |y| < L_y, |z| < d, \tag{11}$$

and zero outside.

The Fourier transform of equation (11) is easily found in terms of $\mathrm{sinc}\,(x) \equiv (\sin x)/x$ functions, namely

$$D(\mathbf{k}) = V_{\mathrm{R}}\,\mathrm{sinc}\,(L_x k_x)\,\mathrm{sinc}\,(L_y k_y)\,\mathrm{sinc}\,(dk_z), \tag{12}$$

where $V_{\mathrm{R}} = 8L_xL_yd$ is the volume of the rectangular particle.

From the previous expression, together with equations (5), (6) and (10), the vector potential, magnetic induction and phase shift can be calculated. The Fourier transform of the magnetic contribution to the phase shift, for a magnetization forming an angle β with the x axis, then becomes

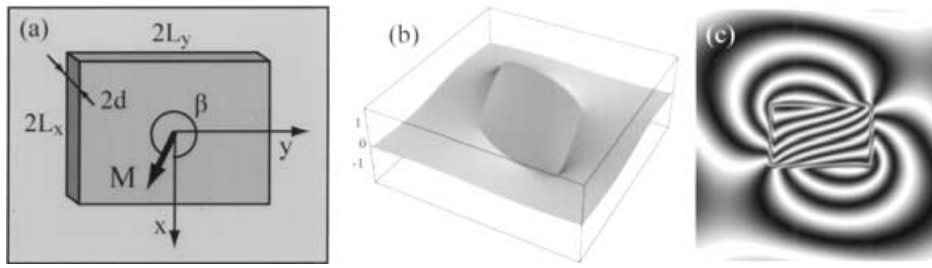

Figure 1. (*a*) Rectangular nanoparticle, coordinate system and main parameters involved; (*b*) purely magnetic phase shift displayed as a three-dimensional plot; (*c*) holographic contour map (amplified 12 times) of the total phase shift $\varphi_e + \varphi_m$.

$$\varphi_m(\mathbf{k}) = \frac{i\pi B_0 V_R}{\phi_0} \frac{k_y \cos\beta - k_x \sin\beta}{k_\perp^2} \operatorname{sinc}(L_x k_x) \operatorname{sinc}(L_y k_y), \tag{13}$$

whose inverse Fourier transform can be in principle calculated analytically.

An example of the magnetic phase shift, calculated from equation (13) by means of an inverse FFT, is shown in figure 1 (*b*) for the following set of parameters: $L_x = 60\,\text{nm}$, $L_y = 100\,\text{nm}$, $d = 10\,\text{nm}$, $\beta = 300°$, $B_0 = 1.6\,\text{T}$ and $V_0 = 10\,\text{V}$.

As the particle surfaces are flat (the projected thickness t_p in equation (9) is a constant), the electrostatic contribution φ_e reduces to a constant term inside the particle, and zero outside. This means that the only effect of the thickness is a phase shift across the particle borders, which is responsible for a discontinuity of the holographic contour fringes displayed in figure 1 (*c*), where the particle shape was slightly smoothed in order to mimic the real specimen edges usually encountered in experiments.

2.2. *Cylindrical geometry*

A cylindrical particle is not very different from the rectangular case, as the electrostatic contribution is still represented by a phase discontinuity on the particle edge. The calculation of the magnetic contribution can be performed by choosing a cylindrical set of coordinates (r, θ, z), and following the steps of the previous section.

For a cylindrical particle of radius R and thickness $t = 2d$, as shown in figure 2 (*a*), the shape function can be defined as

$$D(\mathbf{r}) = 1 \quad \text{for} \quad r < R,\ |z| < d, \tag{14}$$

and zero outside.

Its Fourier transform, which in cylindrical coordinates becomes a Hankel transform owing to the radial dependence of the volume function, is easily evaluated as

$$D(\mathbf{k}) = \frac{2\pi R t}{k_\perp} J_1(k_\perp R) \operatorname{sinc}(dk_z), \tag{15}$$

where $J_1(x)$ is the Bessel function of first order. After integration along the optical axis, the phase shift can be expressed as

$$\varphi_m(\mathbf{k}) = \frac{2i\pi^2 B_0 R t}{\phi_0} \frac{k_y \cos\beta - k_x \sin\beta}{k_\perp^3} J_1(k_\perp R). \tag{16}$$

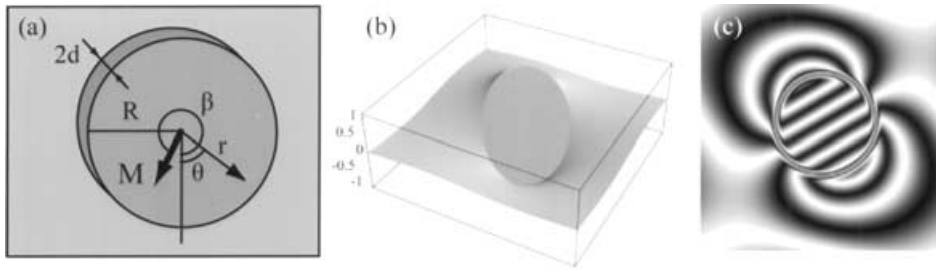

Figure 2. (*a*) Cylindrical nanoparticle, coordinate system and main parameters involved; (*b*) purely magnetic phase shift displayed as a three-dimensional plot; (*c*) holographic contour map (amplified 16 times) of the total phase shift $\varphi_e + \varphi_m$.

Also, in this case the inverse Fourier transform can be computed analytically. As this represents a valuable test of the correctness of the procedure, we have evaluated the inverse Fourier transform of equation (16) and compared it with the phase shift calculated in real space by M. De Graef (2002, private communication), obtaining full agreement. The magnetic phase shift, calculated from equation (16) by means of an inverse FFT, is shown in figure 2 (*b*) for the parameters $R = 50\,\text{nm}$, $d = 10\,\text{nm}$, $\beta = 300^\circ$, $B_0 = 1.6\,\text{T}$ and $V_0 = 10\,\text{V}$. The effect of the electrostatic phase shift is shown in figure 2 (*c*) and, as before, it reveals itself only near the particle edges.

2.3. *Spherical geometry*

A spherical particle is rather different from the previous configurations. The basic difference is in the electrostatic contribution, which has a dramatic effect on the total phase shift as there are no flat surfaces on a sphere. Moreover, as the ratio of the two contributions depends on the sphere radius, as will be shown in the following section, for very small particles under 50 nm in radius, the magnetic signal is masked by the predominant electrostatic signal. This is even more striking when the sphere is in the vortex state, as the two contributions are similar not only in amplitude but also in shape.

Let us consider a spherical particle of radius R and perform the analysis in spherical coordinates (r, θ, ϕ). The shape function is simply

$$D(\mathbf{r}) = 1 \quad \text{for} \quad r < R, \tag{17}$$

and zero for $r > R$, while its Fourier transform is

$$D(\mathbf{k}) = \frac{4\pi R^2}{k}\, j_1(kR), \tag{18}$$

where $j_1(x) = (\operatorname{sinc} x - \cos x)/x$ is the spherical Bessel function of first order. The phase shift is then

$$\varphi_m(\mathbf{k}) = \frac{4\pi^2 i B_0 R^2}{\phi_0}\, \frac{k_y \cos\beta - k_x \sin\beta}{k_\perp^3}\, j_1(k_\perp R). \tag{19}$$

The magnetic phase shift, calculated from equation (19) by means of an inverse FFT, is shown in figure 3 (*b*) for the following set of parameters: $R = 50\,\text{nm}$, $\beta = 300^\circ$ and $B_0 = 1.6\,\text{T}$. Once again, the electrostatic component φ_e is added in figure 3 (*c*). Unlike the geometries considered previously, the effect of the electrostatic potential in a spherical particle changes dramatically the projected potential

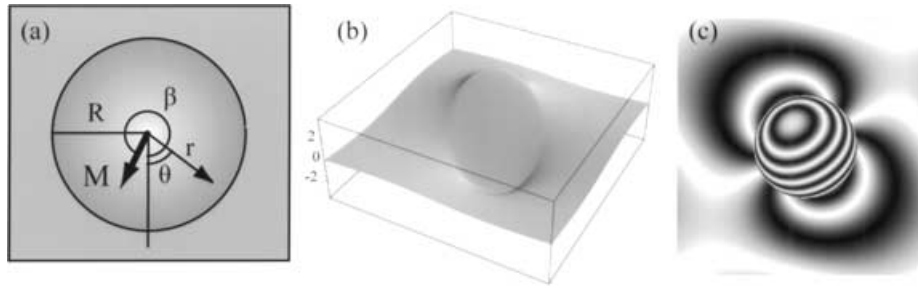

Figure 3. (*a*) Spherical nanoparticle, coordinate system and main parameters involved; (*b*) purely magnetic phase shift displayed as a three-dimensional plot; (*c*) holographic contour map (amplified three times) of the total phase shift $\varphi_e + \varphi_m$.

configuration. As the spherical geometry is the most widely found in self-assembled nanoparticles, the separation of the electrostatic and magnetic contributions to the phase shift represents the major obstacle to a truly quantitative extraction of the magnetic signal. Some more comments on this issue will be given at the end of the following section.

The phase shift derived above for a uniformly magnetized spherical particle is consistent with that described in real space by De Graef *et al.* (1999), thus demonstrating the robustness of our procedure.

§ 3. The vortex state

To describe circular magnetizations, which are frequently found at zero applied field, we have to modify the approach slightly. While the basic equation (1) remains valid, the magnetization unit vector is not a constant any longer, as it is now flowing circularly inside the particle. Therefore, the general considerations employed for a uniform magnetization are not valid, and we have to generalize the approach.

Let us consider a circular flux line carrying an arbitrary number $N_f\phi_0$ of magnetic flux quanta, where N_f is not necessarily an integer number as flux quantization does not apply here. If we obtain a solution for the vector potential, and then for the phase shift, we can use it to reproduce a realistic magnetic field topography of the circular domain.

The magnetization corresponding to a closed circular flux line of radius R (shown in figure 4 (*a*)), written in cylindrical coordinates, is

$$\mathbf{M} = \frac{N_f\phi_0}{\mu_0}\,[-\sin\theta, \cos\theta, 0]\delta(r-R)\delta(z), \tag{20}$$

where the unit vector $[-\sin\theta, \cos\theta, 0]$, describing a counterclockwise flux flow, has the role previously assumed by $\hat{\mathbf{m}}$. Its Fourier transform is directly obtained as

$$\mathbf{M}(\mathbf{k}) = \frac{2\pi i N_f\phi_0 R}{\mu_0}\,\frac{J_1(k_\perp R)}{k_\perp}\,[-k_y, k_x, 0]. \tag{21}$$

We can now calculate the vector potential, by means of equation (2), and integrate along the electron trajectory to obtain the phase shift

$$\varphi_m(\mathbf{k}) = -2\pi^2 N_f R\,\frac{J_1(k_\perp R)}{k_\perp}. \tag{22}$$

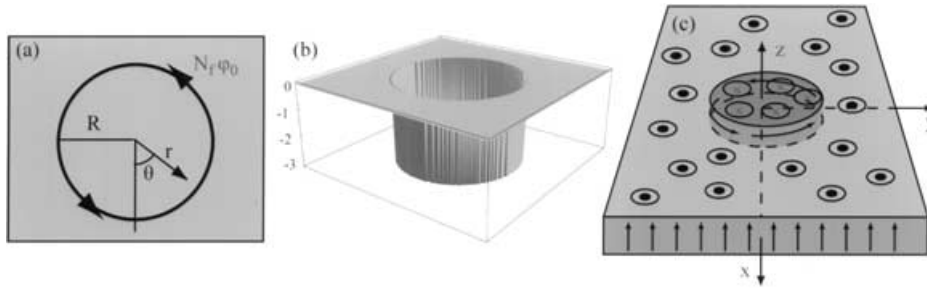

Figure 4. (*a*) Circular flux line carrying N_f flux quanta; (*b*) resulting magnetic phase shift; (*c*) physical situation represented by the model.

This expression can be inverted to real space:

$$\begin{aligned}\varphi &= -\pi N_f R \int_0^{+\infty} \mathrm{d}k\, J_1(kR) J_0(kr) \\ &= \begin{cases} -\pi N_f, & r < R, \\ 0, & r > R, \end{cases}\end{aligned} \tag{23}$$

which is a cylinder of radius R, and height $-\pi N_f$, as shown in figure 4 (*b*).

This result can be employed to describe the phase shift of a cylindrical particle of uniform vertical magnetization, embedded in a medium of opposite magnetization, as shown in figure 4 (*c*).

3.1. *Domain wall widths*

We can extend our result to a realistic domain structure by describing the flux distribution across a Bloch domain wall with a suitable function $\phi(r)$. For instance, it has been suggested by Mansuripur (1995) that a suitable wall description is provided by

$$\cos[\theta(r)] = \tanh\left(\frac{r-R}{\Delta}\right), \tag{24}$$

where θ represents the angular change of the magnetization unit vector across the Bloch wall (from 0° to 180°), and Δ is equal to $(A/K)^{1/2}$, with A the exchange coefficient and K the anisotropy constant of the material. Following the considerations made by Hubert and Schäfer (1998), we can define the wall width as $W = \pi\Delta$.

Resorting to numerical procedures, we can evaluate the Fourier transform of the function

$$\phi(r) = \sin[\theta(r)] = \operatorname{sech}\left(\frac{r}{\Delta}\right) \tag{25}$$

and compute the convolution $\varphi_{\mathrm{tot}}(\mathbf{k}) = \varphi(\mathbf{k})\phi(\mathbf{k})$ in order to include the effect of the wall width on the phase shift. The plots of the phase shift corresponding to the three different values $\Delta = 1$, 5 and 10 nm are shown in figure 5.

The sensitivity of the phase shift to domain wall structures may enable various physical properties of magnetic materials to be directly determined through the measurement of the domain wall width.

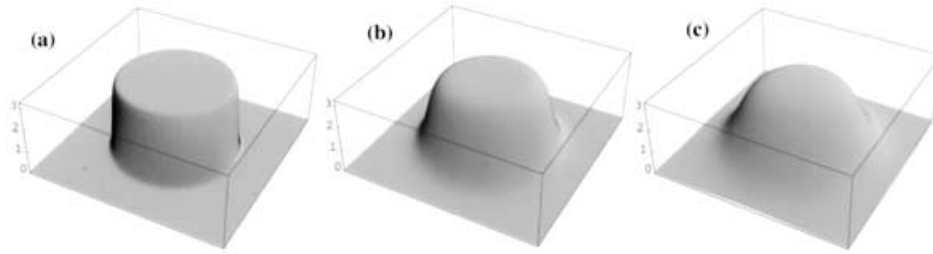

Figure 5. Magnetic phase shift of a circular domain calculated for $N_f = 1$ and for different values of the wall width: (*a*) 1 nm; (*b*) 5 nm; (*c*) 10 nm.

3.2. *Vortex state of nanoparticles*

Using the same formalism, we can generalize the previous results to a circularly magnetized disc of radius R and thickness t, for which the phase shift in real space is

$$\varphi_m = \frac{\pi B_0 t}{\phi_0}(R - r), \tag{26}$$

to a circularly magnetized sphere of radius R:

$$\varphi_m = \frac{\pi B_0 R}{\phi_0}\left\{R \arcsin\left[\left(1 - \frac{r^2}{R^2}\right)^{1/2}\right] - r\left(1 - \frac{r^2}{R^2}\right)^{1/2}\right\}. \tag{27}$$

Extending the approach to a non-circular closed flux line on a rectangular domain, in which the geometry induces the formation of 90° domain walls (with the assumption of zero wall width), gives

$$\varphi_m = \frac{\pi B_0 t}{\phi_0} \min\left\{\begin{matrix} L_x - |x| \\ L_y - |y| \end{matrix}\right\}. \tag{28}$$

Since any enclosed flux structure has no fringing fields, in the previous three expressions the phase shift outside the particle is identically zero. The situations are depicted in figure 6.

It is of importance to compare the electrostatic and magnetic contributions with the phase shift in a circularly magnetized spherical particle, as this can give useful hints on the capabilities of TEM to retrieve a magnetic signal from nanoparticles.

The electrostatic and magnetic contributions to the phase shift strongly depend on the particle radius. If we choose a favourable condition for the observation, that is a reasonably high accelerating voltage (300 kV), and an embedding medium with

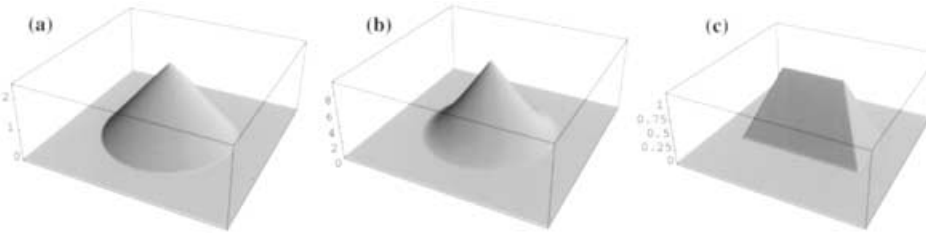

Figure 6. Vortex state of the magnetization in (*a*) a cylindrical nanoparticle, (*b*) a spherical nanoparticle and (*c*) a rectangular nanoparticle.

a mean inner potential not very different from that of the magnetic particle (e.g. $V_0 = 10\,\mathrm{V}$), we can plot φ as a function of the particle radius R (figure 7 (*a*)). We can define the characteristic radius $R_c = 4\phi_0 V_0/\pi\lambda E B_0 = 34\,\mathrm{nm}$, for which electrostatic and magnetic contributions are equal. For smaller R, the electrostatic contribution is predominant and overwhelms the magnetic phase, which reaches the limit of detectability (here assumed equal to $\pi/20$) around $R = 7\,\mathrm{nm}$, as displayed in figure 7 (*b*).

For a spherical particle of radius $R = R_c/2 = 17\,\mathrm{nm}$ the magnetic signal can be considered as a perturbation with respect to the predominant electrostatic phase shift shown in figure 7 (*e*). This poses a serious limitation in the TEM usefulness for magnetic observations. However, with a careful choice of the experimental set-up and specimen geometry, it is possible to reach the now inaccessible region under R_c.

The assumed limit of detectability $\pi/20$ is actually very dependent on the experimental set-up, and on the phase retrieval technique employed. As electron holography is generally claimed to be a technique capable of retrieving the phase shifts as small as $\pi/100$ (Tonomura 1993), in principle there is no lower limit for extracting the magnetic signal for nanoparticles with TEM, as $\pi/100$ corresponds to a particle radius smaller than 3 nm, which is very close to the atomic scale. Certainly, the electrostatic contribution should be precisely taken into account first, otherwise the real limit for magnetic observation in TEM remains R_c. A thorough analysis of the problems involved in the separation of the magnetic and electrostatic components by *in-situ* magnetization reversal was given by Dunin-Borkowski *et al.* (1998).

Our Fourier space approach can be extended to the case of tilted specimens. This may determine whether the problem of the separation of the electrostatic and magnetic components is solved, and as an additional advantage it allows us to extract information on the vertical component of the magnetic field. With a slight modifica-

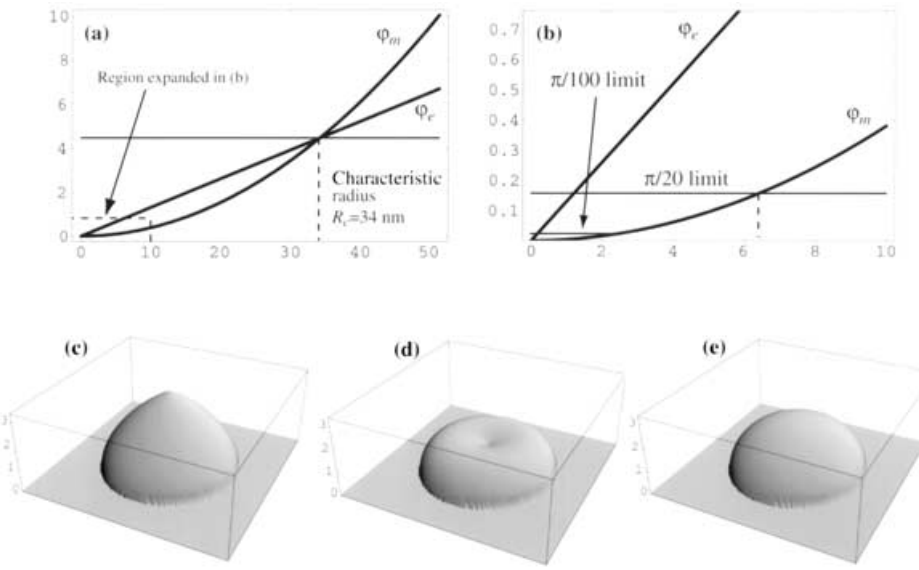

Figure 7. (*a*) Comparison between the electrostatic and magnetic components of the phase shift in a spherical particle; (*b*) expansion of the region around $R = 0$ to emphasize the detectability limits; (*c*) total phase shift, clockwise magnetization; (*d*) total phase shift, counterclockwise magnetization; (*e*) electrostatic component of the phase shift for a spherical particle of radius $R = R_c/2 = 17\,\mathrm{nm}$.

tion of equation (8), namely integrating along a tilted trajectory, we can obtain new expressions for the magnetic (equation (10)) and electrostatic (equation (9)) components of the phase shift for a generic specimen tilt angle. More details, and the actual analytical expressions, will be given in the companion paper, part II (Beleggia *et al.* 2003).

§4. Arrays of nanoparticles

An advantage of having a Fourier representation of the phase shift is its straightforward extension to arrays of nanoparticles. Assuming that the specimen under observation is made of a regular array of dots, or discs, or bars (spherical, cylindrical or rectangular geometries respectively), each element is located by a standard Bravais lattice vector $\mathbf{r}_j$. The total phase shift for the array composed of N elements, each of them having a phase shift φ_j, can be written in real space as

$$\varphi_{\mathrm{tot}}(\mathbf{r}) = \sum_{j=1}^{N} \varphi_j(\mathbf{r} - \mathbf{r}_j), \tag{29}$$

which in Fourier space becomes

$$\varphi_{\mathrm{tot}}(\mathbf{k}) = \sum_{j=1}^{N} \varphi_j(\mathbf{k}) \exp(-\mathrm{i}\mathbf{r}_j \cdot \mathbf{k}), \tag{30}$$

that is a Fourier series composed of N terms.

As this issue will be treated extensively in part II, let us just give a simple example here: an array composed of four rectangular elements with different aspect ratios, as shown in figure 8 (*a*). Each element has the same $\hat{\mathbf{m}}$ unit vector, oriented at an angle $\beta = 45^\circ$. While the electrostatic component is still only responsible for the discontinuity of the holographic fringes at each element edge, as shown in figure 8 (*b*), the magnetic phase shift is now giving information about the interaction between the elements. Phase contour lines are going from one element to another, revealing that the local field inside one rectangle is influenced by the nearby elements.

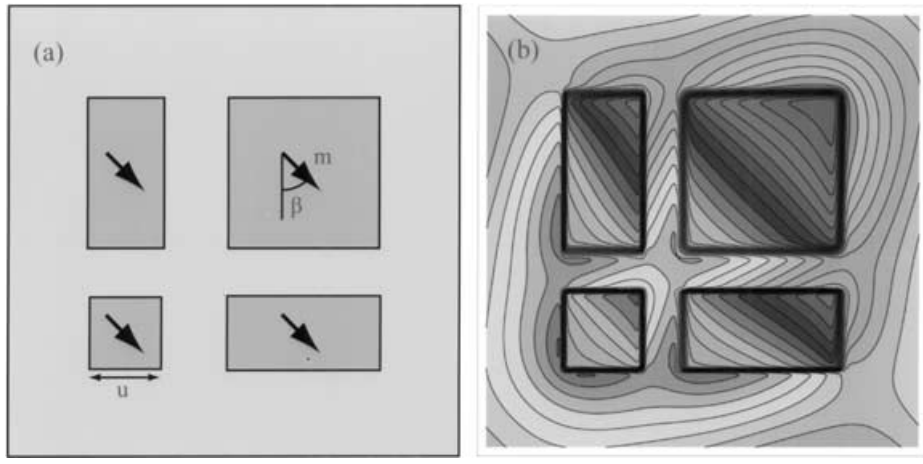

Figure 8. (*a*) Array of four rectangular elements with various aspect ratios (1 : 1, 1 : 2, 2 : 1 and 2 : 2), where the element unit size u in the figure is 50 nm; (*b*) contour line plot of the total phase shift $\varphi_{\mathrm{e}} + \varphi_{\mathrm{m}}$ (each line represents a phase shift of $\pi/4$).

Moreover, we can extract some information on the effect of the demagnetizing field. In fact, the contour lines within the rectangular elements appear to be oriented in a direction which is not exactly parallel to the magnetization unit vector. They appear to be tilted at an angle which depends on the aspect ratio of the element. This is the combined effect of the projection of the magnetic field along the beam direction, typical of any TEM experiment, and of the demagnetizing field generated by each element of the array. Whenever fringing fields are involved, which means every time that an element is not in the vortex state, it is not yet possible to retrieve the actual 'induction map' (i.e. the B field in the specimen plane) from the phase shift alone. Therefore, one has to be very careful to interpret holographic contour maps as induction maps. This subject will be investigated in greater detail in part II.

§ 5. Conclusions

We have shown that a complete theoretical framework is now available for the interpretation of TEM observations of magnetic nanoparticles. The Fourier space approach employed in this paper enables analytical calculation of magnetic fields and structures that were only numerically feasible up to now. The calculation scheme presented here has a wide range of applications in the analysis of experiments involving characterization of magnetic structures on the nanometre scale. An approach to more complicated particle geometries will be presented in the companion paper, part II (Beleggia *et al*. 2003), where the huge class of facetted particles (including the five Platonic and 13 Archimedean solids) will be described analytically. Moreover, the magnetization, which is now considered as a superimposed parameter, should be derived from energy minimization. Loosening the constraint of analytical calculation, which cannot go beyond the uniform or circular magnetization, we can take into account more realistic topographies, such as multiple-domain structures or non-uniform single domains. Work in this direction is in progress.

Acknowledgements

We gratefully acknowledge the useful discussions with Professor M. De Graef (Carnegie Mellon University, USA) and Professor G. Pozzi (University of Bologna, Italy), as well as the contribution to the completion of this work given by Dr M. A. Schofield and Dr V. V. Volkov. This work was supported by Division of Materials Sciences, Office of Basic Energy Science, US Department of Energy, under contract DE-AC02-98CH10886.

References

Aharonov, Y., and Bohm, D., 1959, *Phys. Rev*., **115**, 485.
Beleggia, M., Fazzini, P., and Pozzi, G., 2002, *Ultramicroscopy* (in press).
Beleggia, M., and Pozzi, G., 2000, *Ultramicroscopy*, **84**, 171; 2001, *Phys. Rev*. B, **63**, 4507.
Beleggia, M., Tandon, S., Zhu, Y., and De Graef, M., 2003, *Phil. Mag*. (in press).
Chapman, J., 1984, *J. Phys*. D, **17**, 623.
De Graef, M., 2001, *Magnetic Microscopy and its Applications to Magnetic Materials*, edited by M. De Graef and Y. Zhu (New York: Academic Press), chapter 2, pp. 27–67.
De Graef, M., Nuhfer, N., and McCartney, M., 1999, *J. Microsc*., **194**, 84.
Dunin-Borkowski, R. E., McCartney, M. R., Smith, D. J., and Parkin, S., 1998, *Ultramicroscopy*, **74**, 61.
Gomez, R., 2001, *Magnetic Microscopy and its Applications to Magnetic Materials*, edited by M. De Graef and Y. Zhu (New York: Academic Press), chapter 3, pp. 69–110.
Hubert, A., and Schäfer, R., 1998, *Magnetic Domains* (Berlin: Springer).
Jackson, J. D., 1975, *Classical Electrodynamics* (New York: Wiley).

MANSURIPUR, M., 1995, *The Physical Principles of Magneto-optical Recording* (Cambridge University Press).
PAGANIN, D., and NUGENT, K., 1998, *Phys. Rev. Lett.*, **80**, 2586.
TONOMURA, A., 1993, *Electron Holography* (Berlin: Springer).
UNGURIS, J., 2001, *Magnetic Microscopy and its Applications to Magnetic Materials*, edited by M. De Graef and Y. Zhu (New York: Academic Press), chapter 6, pp. 167–194.